Identification of Kinesin Neck Region as a Stable α-Helical Coiled Coil and Its Thermodynamic Characterization

Hisayuki Morii,*,§ Tatsuyuki Takenawa,§ Fumio Arisaka,|| and Takashi Shimizu§,⊥

National Institute of Bioscience and Human-Technology, Tsukuba, Ibaraqi 305, Japan, Tokyo Institute of Technology, Midori, Yokohama 222, Japan, and National Institute for Advanced Interdisciplinary Research, Tsukuba, Ibaragi 305, Japan

Received September 23, 1996; Revised Manuscript Received December 4, 1996⊗

ABSTRACT: The kinesin heavy chain consists of an N-terminal globular domain, referred to as the motor domain, a rod-like middle region, and a C-terminal domain. In this study, the human kinesin neck region, the region adjacent to the motor domain which promotes dimerization, has been investigated. First, we predicted coiled-coil regions including the neck region by our newly devised statistical method. The sequence (335−372) was predominated by a unique heptad amphipathy. A comparison of the bacterially expressed human kinesin heavy chain fragments, K349 (1−349), a monomeric motor domain, and K379 (1−379), a dimer, by circular dichroism (CD) spectroscopy showed that K379 had more α-helical content. Chemically synthesized peptides, (332−349), (350−379), and (332-369), gave CD spectra with an α-helix-rich pattern, but the spectra varied depending on the peptide concentration. Analysis of the molar ellipticity at 222 nm indicated that those peptides were in monomer−dimer equilibria, and the dissociation isotherms established dissociation constants of 9.6 mM, 60 μM, and 62 nM for the above peptides, respectively. Sedimentation equilibrium measurements verified that the peptide (332−369) existed as a dimeric form. These results strongly suggest that the sequence from 332 to 369 of the neck region forms an α-helical coiled coil. The differential peptide of K349 and K379, (350−379), did not show sufficient ability to make K379 dimeric. It is likely that the region (350−379) forms a stable α-helical coiled coil only together with the (332−349) region. Fluorescence energy transfer studies of [Cys^{363}]-(332−369) labeled with a fluorescence donor and an acceptor revealed that the peptide formed a parallel coiled coil. This coiled coil was thermodynamically stable against urea and thermal denaturation, and peptide exchange of the coiled coil was undetectable, or extremely slow, at neutral pH. The dissociation free energy was estimated to be 57.7 kJ mol^{-1} at a peptide concentration of 22 μM. These results indicate that the neck region of kinesin forms a stable coiled coil which may be important for the motility of dimeric kinesin.

Kinesin is a motor protein with ATPase activity and moves toward the microtubule plus-end by utilizing free energy released upon ATP hydrolysis (Vale et al., 1985, 1996). The structure revealed by rotary shadowing electron microscopy (EM) is somewhat similar to that of skeletal myosin: two globular domains are found at one end of a long rod-like filament, while the other end contains a fan-shaped structure (Hisanaga et al., 1989; Hirokawa et al., 1989). From the deduced amino acid sequence of the heavy chain, the N-terminal 330∼340 amino acid residues form a globular domain of about 40 kDa molecular mass, which corresponds to the globular domains revealed by EM as described above. This domain contains the ATPase site as well as the ATP-dependent microtubule binding site (Yang & Goldstein, 1989). Thus, this domain is called the motor domain.

Recently, numerous kinesin-related proteins have been found (Goldstein, 1993; Bloom & Endow, 1994; Walker et al., 1993). Each member of this kinesin superfamily has a domain homologous to the kinesin motor domain and a nonmotor domain(s) which is rather specific to individual members. Some of the members have been expressed in bacteria or in baculovirus systems and have been shown to have microtubule motor activity.

One very surprising finding was that some members, such as ncd from *Drosophila*, move toward the microtubule minus-end (Walker et al., 1991; McDonald et al., 1991), the direction opposite to that of kinesin itself. How different directions of motion are achieved with homologous motor domains is a very intriguing question. Recent enzymological studies on kinesin and ncd ATPase indicated that their properties are similar to each other (Lockhart & Cross, 1994; Shimizu et al., 1995; Ma & Taylor, 1995a,b). Moreover, X-ray crystallography indicated almost identical core structures for kinesin and ncd motor domains (Sablin et al., 1996; Kull et al., 1996).

So far, many kinesin constructs have been successfully expressed in bacteria with the motor and ATPase activities retained. It has been shown that even fairly short ones, like K379, a human kinesin fragment consisting of amino acid residues 1−379, are not monomeric but dimeric (Hackney, 1994; Correia et al., 1995; Ma & Taylor, 1995a). Thus, the region adjacent to the motor domain seems to have the ability to dimerize, probably by making an α-helical coiled coil. Hackney (1994) showed that the dimeric kinesin construct binds to microtubules with one motor domain while the partner motor domain is dissociated. This has been supported by electron microscopic observations (Hirose et al., 1996), although some opposing evidence has been presented as well

* To whom correspondence should be addressed: Tel, (+81)-298-54-6184; Fax, (+81)-298-54-6194.
§ National Institute of Bioscience and Human-Technology.
|| Tokyo Institute of Technology.
⊥ National Institute for Advanced Interdisciplinary Research.
⊗ Abstract published in *Advance ACS Abstracts,* January 15, 1997.

S0006-2960(96)02392-6 CCC: $14.00

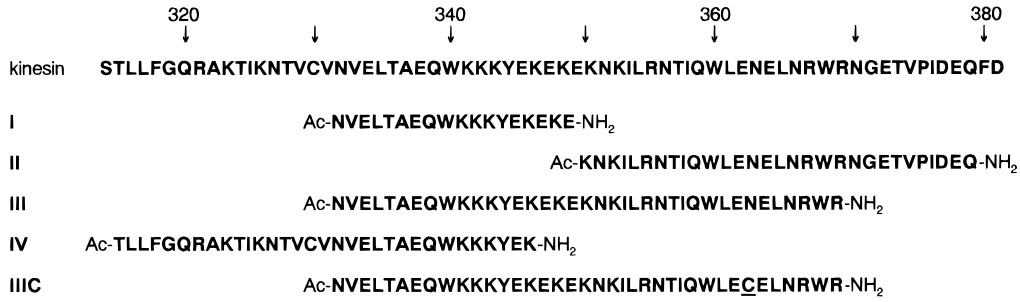

FIGURE 1: Amino acid sequence around the possible neck region of human kinesin heavy chain and the primary structures of chemically synthesized peptides in this work. The amino acid residues are denoted with one-letter abbreviations. N-Terminal Ac and C-terminal NH_2 represent acetylated and amide termini, respectively. The position of cysteine substitution in peptide IIIC is shown with an underline.

(Gilbert et al., 1995). On the basis of these results, Hackney (1994) proposed an intriguing hypothesis that the direction of the dissociated motor domain from the microtubule-bound motor domain depends on the species of kinesin family members, determining the directionality: e.g., the dissociated motor domain of dimeric kinesin points toward the plus-end of microtubule, while that of ncd points toward the minus-end, an equilibrium model for directionality. Thus, the structure of the neck regions of kinesin family members may be of primary importance in the directionality. Unfortunately, however, the recent X-ray crystallographic studies (Sablin et al., 1996; Kull et al., 1996) did not reveal the neck regions of kinesin or ncd, as they were disordered in the structure.

As the first step in the structural studies of the kinesin neck region, we reexamined the secondary structural prediction of kinesin and carried out a spectroscopic investigation of the neck region by syntheses of the corresponding peptides. We also compared the CD spectra of monomeric and dimeric kinesin motor domains, i.e., K349 and K379. Our results indicate that the region 332−369 forms a tightly self-associating dimer, probably α-helical coiled coil.

MATERIALS AND METHODS

Chemicals. Fmoc-amino acids were purchased from Watanabe Chem. Ind. (Hiroshima, Japan). The side chain protection was as follows: Lys(Boc),[1] Ser(tBu), Thr(tBu), Tyr(tBu), Cys(Trt), His(Trt), Asn(Trt), Gln(Trt), Arg(Pbf), Asp(OtBu), and Glu(OtBu). The resin TGS-CHA, purchased from Shimadzu (Kyoto, Japan), was used for solid phase synthesis to provide the peptides with amide-type C-termini. *N*-(9-Acridinyl)maleimide (NAM) and *N*-[*p*-(2-benzimidazolyl)phenyl]maleimide (BIPM) were purchased from Dojin (Kumamoto, Japan) and Teika (Toyama, Japan), respectively.

Preparation of Proteins. Human kinesin fragments K349 and K379 were expressed in *Escherichia coli* and purified as described previously (Ma & Taylor, 1995a; Kull et al., 1996). Briefly, high-speed supernatant of bacterial lysate was fractionated by P-cellulose and Q-Sepharose FF column chromatography, and the resultant peak fractions were passed through an SP-Sepharose FF column.

Synthesis of Peptides. Five peptides (Figure 1) were synthesized by the solid phase method using a Shimadzu PSSM8 peptide synthesizer. The peptides were elongated by a stepwise coupling reaction in each Fmoc-amino acid solution containing a 0.2 M TBTU−HOBt−NMM (1:1:2 equiv) reagent system for 25 min. The peptides were cleaved from the resin with a solution of 90% trifluoroacetic acid, 6% 1,2-ethanedithiol, 3% water, and 1% phenol. Deprotected peptide amides were collected by precipitation with diethyl ether and purified by RP-HPLC on a ShimPack-PREP-C8 column (Shimadzu, Kyoto, Japan) (20 × 250 mm). The peptides were eluted with a linear gradient of acetonitrile in water containing 0.08% trifluoroacetic acid. The purified peptides were shown to be homogeneous (97−99%) by analytical RP-HPLC on an Inertsil-ODS column (GL Sciences, Tokyo, Japan) (4.6 × 250 mm) and were stored in a freezer after lyophilization.

Mass spectrum analysis (ESI-MS) with API-III (Perkin Elmer Sciex Instruments) was carried out to determine the molecular weights of synthesized peptides. The observed molecular weights of peptides I, II, III, and IV were 2321.5 (theoretical value, 2321.5), 3749.2 (3749.2), 4927.6 (4928.4), and 3809.0 (3809.3), respectively. The concentrations of the peptide solutions were determined with the absorbance at 280 nm on the basis of absorption coefficients (Solli et al., 1973).

Fluorescence Labeling of Peptide IIIC. Selective labeling of Cys residue in peptide IIIC, i.e., [Cys^{363}]-(332−369), was achieved with NAM or BIPM as follows. One and one-half micromoles of the purified peptide IIIC having a free thiol group was dissolved in 20 mM phosphate buffer solution (1.7 mL), and the pH was adjusted to 7. Two micromoles of NAM or BIPM in acetone (0.5 mL) was added to start the reaction, and the reaction mixture was stirred at 20 °C for 2.5 h. Then, the reaction was stopped by the addition of excess 2-mercaptoethanol (30 μL). The ring-opening reaction of maleimide ring was carried out by the addition of 1 M NaOH (0.5 mL). After 2.5 h, 0.6 mL of acetic acid was added to bring the pH to 3−4 and the solution was loaded onto an RP-HPLC column for purification as described above. The main peak was collected and lyophilized to obtain a fluorescent-labeled peptide IIIC (IIIC-NAM or IIIC-BIPM). The molecular weights of IIIC-NAM and IIIC-BIPM were determined by ESI-MS to be 5208.2 (theoretical value, 5209.7) and 5225.0 (5224.7), respectively, which indicated that the ring-opened fluorescent maleimide

[1] Abbreviations: Boc, *tert*-butyloxycarbonyl; tBu, *tert*-butyl; Trt, triphenylmethyl; Pbf, (2,2,4,6,7-pentamethyl-2,3-dihydrobenzofuran-5-yl)sulfonyl; OtBu, *tert*-butyloxy (*tert*-butyl ester); NAM, *N*-(9-acridinyl)maleimide; BIPM, *N*-[*p*-(2-benzimidazolyl)phenyl]maleimide; TBTU, 2-(1*H*-benzotriazol-1-yl)-1,1,3,3-tetramethyluronium tetrafluoroborate; HOBt, 1-hydroxybenzotriazole; NMM, *N*-methylmorpholine; Fmoc, 9-fluorenylmethoxycarbonyl; RP-HPLC, reversed-phase high-performance liquid chromatography; ODS, octadecylsilane; ESI-MS, electrosprayed ionization mass spectroscopy; MOPS, 3-(*N*-morpholino)-propanesulfonic acid.

derivatives were attached to the peptide IIIC uniquely as expected.

Circular Dichroism (CD) Measurement. The CD spectra in the far-UV region (196−260 nm, unless otherwise described) were recorded on a Jasco J-600 spectropolarimeter. Cylindrical quartz cuvettes with 0.2−10 mm path length were used, and the temperature was controlled at 20 °C with a water circulation system. The spectral data were collected in a solution of 20 mM MOPS−NaOH (pH 7.0) containing 0.5 M NaCl. For estimation of the secondary structures of K349 and K379, the CONTIN program (Provencher, 1982) was used. The α-helix contents of synthetic peptides were estimated by the method of Chen et al. (1974).

Sedimentation Equilibrium. Sedimentation equilibrium was performed on a Beckman XL-A analytical ultracentrifuge. The solutions contained 20 mM MOPS−NaOH (pH 7.0) and 0.5 M NaCl. The centrifugation was done at 20 °C, and the distributions of peptides II and III within the cells were monitored by the absorbance of the aromatic residues. Partial specific volumes of the peptides were calculated from those of the constituent amino acids to be 0.715 and 0.722 mL/g for peptides II and III, respectively (Lilley, 1985). These values together with the observed density of the buffer solution were used in deriving the apparent average molecular weight of the peptides.

Fluorescence Energy Transfer Measurement. Fluorescence spectra were obtained at 20 °C in 10 mm path length quartz cuvettes using a Shimadzu RF-5000 fluorometer. For fluorescence measurements a solution of 50 mM potassium phosphate (pH 7.0) was used, because high salt, 0.5 M NaCl, used for CD measurements may act as a quencher of the fluorescence. Although the ingredients in solutions were different from those for CD measurements, CD spectra of the peptides were nearly identical in both solutions. IIIC-BIPM and IIIC-NAM were used as a fluorescence donor and an acceptor of energy transfer system, respectively. The concentration of fluorescently labeled peptides was roughly estimated by subtracting the spectra of BIPM-labeled (or NAM-labeled) cysteine from that of IIIC-BIPM (or IIIC-NAM), but since the fluorescently labeled IIIC's gave the same CD spectra as peptide III, the concentration based on the molar ellipticity at 222 nm was adopted for further studies. Fluorescence spectra were recorded in the range 320−500 nm with an excitation wavelength of 310 nm. The band widths were set to 3 nm for excitation and 5 nm for emission. In order to suppress the inner filter effect, the optical density at the excitation wavelength was set to 0.06 or less by adjustment the concentration.

IIIC-BIPM and IIIC-NAM were dissolved in a small amount of water together and incubated for 20 min at room temperature, and the mixture was diluted with 50 mM potassium phosphate (pH 7.0). By comparing the spectra of the mixture and IIIC-BIPM alone, we calculated the energy transfer efficiency, E_T, from the maximal emission intensity of the BIPM group at 362 nm. Fluorescence energy transfer was analyzed on the basis of Förster's equation (Förster, 1948):

$$R_0 = \kappa^2 \beta n^{-4} \phi_D J$$

where R_0 is the distance at which the transfer efficiency is 0.5; κ^2, the orientation factor for a dipole−dipole interaction; β, a constant; n, the refractive index of the medium taken as 1.4 (Stryer, 1978); ϕ_D, the quantum yield of the donor in the absence of the acceptor; and J, the spectral overlap integral of donor fluorescence and acceptor absorption. The quantum yield of the donor was determined to be 0.037 by comparison with the standard, tryptophan in water. The value of κ^2 was taken as $^2/_3$ on the assumption of free rotation of both donor and acceptor.

Denaturation Experiments. Denaturation curves monitored by CD and fluorescence emission were obtained by the titration of peptide III with urea solution containing 20 mM MOPS−NaOH (pH 7.0) and 0.5 M NaCl at 20 °C. CD was measured at 222 nm. Fluorescence measurement was performed with the excitation at 275 nm, and the spectra in the range 285−400 nm were recorded. The data were plotted for several emission wavelengths in order to detect the individual behaviors of single tyrosine and three tryptophan residues in the peptide.

Thermal denaturation of peptide III was measured by CD as the temperature was increased at a rate of 0.8 K/min. The change was monitored by the ellipticity at 222 nm.

RESULTS AND DISCUSSION

Prediction of Coiled-Coil Domains. The mid-region of kinesin heavy chain is known to form α-helical coiled coil (Yang et al., 1989; de Cuevas et al., 1992). Here we reexamined coiled-coil-forming regions. In order to survey and localize the coiled-coil-forming regions, as well as to discuss the detailed features of the sequence, the prediction of amphipathic helix involving the heptad assignment was performed by our novel method described in the Appendix (Figure 2). Lupas et al. (1991) and later Berger et al. (1995) proposed methods for the prediction of coiled coils, which were based on the natural occurrence of amino acid residues in known coiled coils. On the other hand, our method is based on the thermodynamic parameters of residues, so that it can estimate amphipathic helices, including coiled coils, more generally even though the peptide is composed of non-natural amino acids.

Six major regions and several shorter ones were predicted (Table 1). The major coiled-coil-forming regions, R1−R6, were essentially consistent with those obtained by the method of Lupas et al. (1991), which were the (331−371), (411−541), (596−695), (727−802), and (821−904) regions, though their fourth region corresponded to our R4 and R5. Interestingly, the assignments of heptad frame shift were different from each other between any two neighboring major regions; for example, R1 is $7N-6$ while R2 is $7N-2$ (see Appendix for heptad frame shifts). This means that each presumed coiled-coil region is likely an independent domain. From X-ray and motility studies, it has been revealed that an N-terminal region of about 330∼340 residues forms the globular head of kinesin. Consequently, therefore, we could assume that the first sequence, R1 (335−372), would be the neck region by forming a coiled-coil domain.

The fine profile for coiled-coil-forming ability around this region is shown in Figure 2B. The possible type of heptad frame shift was $7N-6$ in the region (335−372). There existed two short domains, (318−331) and R10 (374−389), neighboring to R1. They could be assigned different types of heptad frame shifts, $7N$ and $7N-5$; they might form short and independent coiled coils (however, see below). The

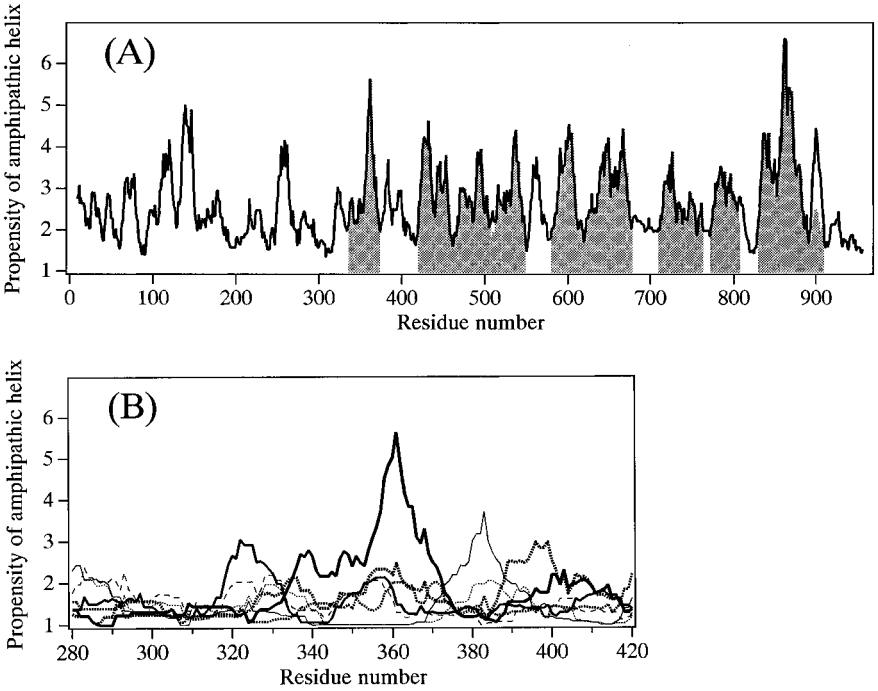

FIGURE 2: (A) Propensity of amphipathic helix formation of human kinesin heavy chain. The sequence was taken from Swiss-Prot accession: P33176. The ordinate corresponds to the propensity score, *w*, at the central position of the 15-residue window (see Appendix). The maximum score among the scores for seven heptad frame shifts is shown at each position with a solid line. The major predicted coiled-coil regions, R1−R6, are shown with hatched bands which indicate the values for their predominant frame shifts. (B) Fine profile of amphipathic helical propensity around the possible neck region. The propensity scores are shown for all seven types of heptad frame shift: 7*N*, medium solid; 7*N*−1, thin dotted; 7*N*−2, medium dotted; 7*N*−3, bold dotted; 7*N*−4, dashed; 7*N*−5, thin solid; and 7*N*−6, bold solid.

Table 1: Predicted Amphipathic α-Helical Regions of Kinesin

residue	residue number[a]	chain length	type of heptad frame[b]
R1	335−372	38	7*N*-6
R2	420−547	128	7*N*-2
R3	580−677	98	7*N*-1
R4	709−762	54	7*N*-5
R5	772−806	35	7*N*-2
R6	829−908	98	7*N*-1
R7[c]	105−129	25	7*N*
R8	129−151	23	7*N*-1
R9	247−270	24	7*N*-1
R10	374−389	16	7*N*-5
R11	553−569	17	7*N*-5
R12[d]	893−909	17	7*N*-4

[a] To pick up sequential regions forming stable coiled-coil structures, we set several restraints as follows: (i) ignoring short sequences less than 14 residues long, (ii) picking up a sequence having a score over 3.0 in it (for predicting scores, see Appendix), and (iii) setting a threshold score determining both ends of each region as 2.0. [b] The type of heptad frame shift is represented with the residue number assigned to *a* position (see Appendix). The number 7*N* denotes a multiple of seven. [c] Regions longer than 30 residues are listed in the upper half and the others, in the lower half. [d] The region R12 overlaps with R6.

profile of the region R1 (335−372) was not simple: that is, the trailing half had a higher score than the leading half according to our evaluation method. Moreover, this region contains hydrophilic residues (Glu^{347} and Asn^{351}) at the core of the coiled coil (Figure 3). The sequence from Glu^{345} to Lys^{352} is fully hydrophilic, and most residues are charged ones as seen in the helical network diagram (Figure 3). This region, (345−352), might cause instability or form a hinge of coiled-coil structure, although (332−369) was found to be very stable (see below).

Comparison of CD Spectra of K349 and K379. Figure 4 shows the CD spectra of K349 and K379 in the far-UV region (196−260 nm) in 0.5 M NaCl. While the spectra were similar to each other, the troughs at both 208 and 222 nm were deeper with K379. By the CONTIN simulation program (Provencher, 1982), α-helix, β-structure and the remainders were estimated to be 30%, 35%, and 35% for K349 and 34%, 33%, and 33% for K379, respectively. The higher content of α-helix in K379 is reflected in the deeper troughs in the spectra. The difference in the secondary structure estimations could be explained if the differential segment (350−379) would form an α-helix and the C-terminus region of K349, which would not be α-helical in K349, would form an α-helix in K379. The inset of Figure 4 indicates the difference spectrum of K349 and K379. The molar ellipticity of this segment at 222 nm was -35000 ± 6000 deg cm^2 dmol^{-1} (the error range corresponds to the error of 2% in the protein concentrations). According to the quantitative estimation proposed by Chen et al. (1974), the difference in α-helical chain length between K349 and K379 was 29 ± 5 residues long. These data were obtained in the presence of high salt, but the spectral patterns were basically the same in the presence of low salt, 0.1 M NaCl, suggesting that the structure of this segment (350−379) as well as other parts would be stable irrespective of the salt concentration.

Self-Association of Human Kinesin Fragments. As mentioned above, the segment (350−379) seemed likely to play an important role to make K379 dimeric, while K349 devoid of this segment is monomeric (Kull et al., 1996). Thus, the peptide fragment (350−379), peptide II, was chemically synthesized to investigate its physicochemical nature. The N- and C-termini were modified to be acetylated and amide

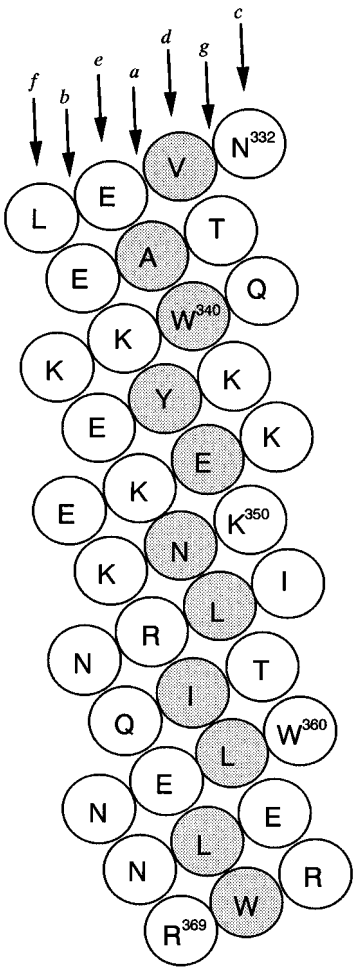

FIGURE 3: Representation of α-helical network of the region (332−369). Every residue is aligned to form α-helix, and its expanded side face is exhibited. The shaded circles represent core positions, and the others are outfield ones. The sequence is assigned to the heptad type 7*N*−6. The residues assigned to the same heptad notation, *a*−*g*, are in line as shown by the arrows above.

(CONH$_2$) form, respectively, to prevent the influence of charged termini on the structure. The fragment (332−369), peptide III, with the same terminal groups was also synthesized. Since the hydrophobic core residues were counted from Val^{333} to Trp^{368} in the region R1 predicted in the previous section, the region (332−369) containing the neighboring residues of these two was selected as peptide III in place of (335−372) (Figure 3). In addition, the differential part of these two fragments, the fragment (332−349), peptide I, and its elongated fragment (315−346), peptide IV, were also prepared (Figure 1).

Self-association of these fragments was investigated by measurement of the concentration dependence of their CD spectra. Peptides I, II, and III exhibited CD spectra typical of α-helix-rich peptides at high concentrations (Figure 5A). When the concentrations were decreased, the CD spectra changed to patterns of disordered secondary structure with shallower troughs at 222 nm and intensive negative bands around 200 nm. These results indicate that these peptides form α-helical structures by self-association. Since the spectral changes had isosbestic points at 203 nm (not shown), they seemed to undergo a two-state transition. The CD intensity at 222 nm was then plotted against the peptide concentration (Figure 5B). The data obtained could be fitted well to curves of monomer−dimer equilibrium and fitted

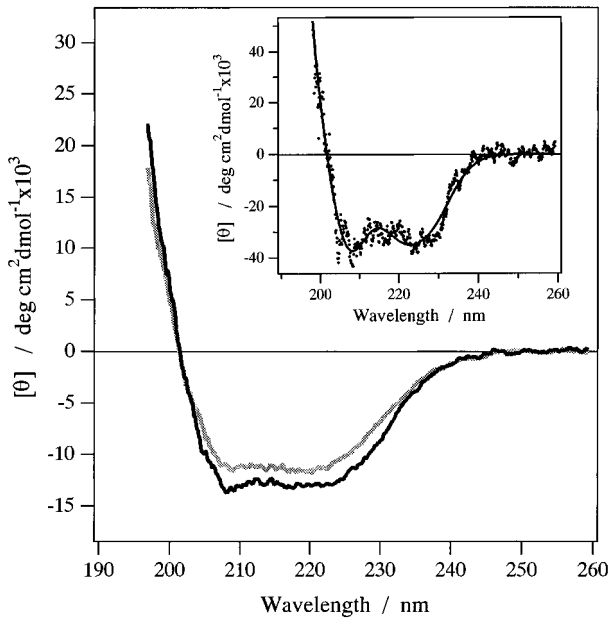

FIGURE 4: Circular dichroism spectra of K349 and K379. Far-UV CD spectra of K349 (shaded line) and K379 (solid line) were measured in 20 mM MOPS buffer (pH 7.0) containing 0.5 M NaCl and 2 mM $MgCl_2$. The inset represents the differential spectrum (dots) of K349 and K379, whose intensity was converted to the molar ellipticity of the differential 30 residues. The differential spectrum was fitted with the curve (solid line) calculated by summation of Gaussian curves by the method of Chen et al. (1974).

poorly to a trimer−monomer (or tetramer−monomer) model. Therefore, these peptides likely form dimeric α-helices at high concentrations, most likely, α-helical coiled coils.

On the other hand, the CD spectra of peptide IV, (315−346), did not show any α-helical pattern (data not shown). The molar ellipticity changed drastically from −5000 to −1000 deg cm^2 dmol^{-1} at about 20 mM; above this concentration, gelation occurred. Although peptide I was likely to have an ability to form an α-helical dimer, peptide IV containing the same sequence as peptide I did not form an α-helix. The N-terminus half of peptide IV might have a propensity for β-structure and result in gel formation at higher concentrations, although Kull et al. (1996) indicate that (306−320) of K349 is α-helical.

The dissociation constants, K_d, obtained by curve-fitting calculations, were 9.6 ± 2.8 mM, 60 ± 31 μM, and 62 ± 31 nM for peptides I, II, and III, respectively. It is noted that peptide II, which has the sequence corresponding to the difference between K349 and K379, had insufficient ability to maintain K379 in a dimeric form at concentrations used for motility and enzymological assays (μM order). On the other hand, peptide III exhibited sufficient ability to make K379 dimeric. The chain length of α-helix was estimated by the equation of Chen et al. (1974), i.e., $[\theta]_H^n = [\theta]_H^\circ(1 - k/n)$, where $[\theta]_H^\circ$ and k are given as −39 500 deg cm^2 dmol^{-1} and 2.57 for the CD intensity at 222 nm. With an assumption that these peptides had no β-structure, the helical chain lengths were calculated to be 21 and 30 residues for peptides II and III, respectively. If the α-helical part of peptide III was separated into two parts due to the cluster of charged amino acid residues from 345 to 352 (see above), the total chain length would be 34 residues; (332−345) and (350−369). The highly hydrophilic sequence (345−352) in this region might be thought to interfere with the continuity

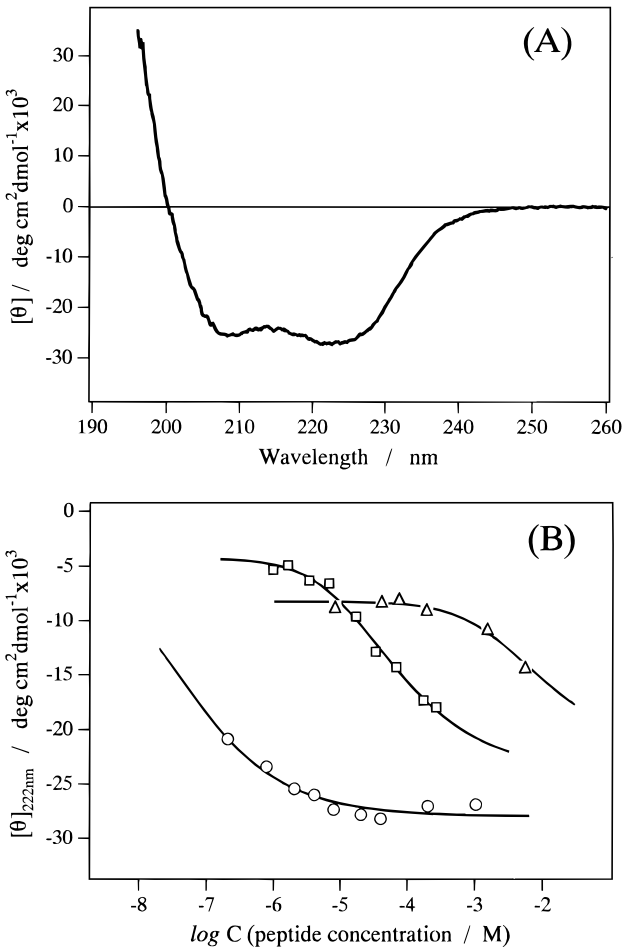

FIGURE 5: (A) Circular dichroism spectrum of peptide III. The spectrum was recorded at a peptide concentration of 0.20 mM in 20 mM MOPS (pH 7.0) in the presence of 0.5 M NaCl. (B) Concentration dependence of the molar ellipticity for the synthetic peptides I−III. CD spectra were measured using the cuvettes with path lengths of 0.2, 0.5, 1, 2, 5, 10, and 20 mm depending on the peptide concentration. The molar ellipticity at 222 nm of peptide I (332−349) (triangles), peptide II (350−379) (squares), and peptide III (332−369) (circles) were plotted against the common logarithm of peptide concentrations. The sigmoidal curves (solid lines) are the fits on the assumption of monomer−dimer equilibrium. The calculation was carried out with the software Igor on a Macintosh PC to fit to the equation $[\theta] = [\theta]_d + ([\theta]_m - [\theta]_d)[\{1+(8C/K)\}^{1/2} - 1](K/4C)$, where $[\theta]_m$, $[\theta]_d$, K, and C denote molar ellipticity of monomer, that of dimer, dissociation constant, and peptide concentration, respectively. The dissociation constants were estimated to be 9.6 mM, 60 μM, and 62 nM for peptides I, II, and III, respectively.

of the α-helix (however, see the last part of Results and Discussion).

One interpretation of these results is that both sequences of peptides I and II were essential for the dimer formation of K379. In other words, either one would not have sufficient ability to form a coiled coil, but they would do so synergetically. The neighboring sequences, (315−331) and (370−379), would have little, if any, effect on the dimerization from the results on these peptides. It should be noted that the possibility that they would contribute to the dimerization in the intact protein could not be excluded.

Generally, electrostatic interaction between an intermolecular *e*−*g* pair has a supplemental effect on the formation of a coiled-coil structure (Adamson et al., 1993), although it should be of little importance in our present case because of high salt conditions.

Sedimentation Equilibrium of the Peptide Fragments. By using an analytical ultracentrifuge, the sedimentation equilibrium data were collected for peptides II and III. The peptide III at a concentration of 50 mM was shown to have an apparent molecular weight of 9613, which was very close to twice the molecular weight for the monomer, 4922. On the other hand, the data of peptide II was not able to be fitted to a theoretical curve for a single component even at a high concentration (e.g., 0.45 mM). In the concentrated region in the centrifuge cell, the apparent molecular weight of peptide II was estimated to be 6426, which would correspond to its 1.7mer. This suggests that peptide II was an equilibrium mixture of the monomer and self-associated species under the conditions of measurement.

Since any higher order oligomers other than a dimer were not observed, it would be natural to assume that this experiment provides direct evidence that peptide III, (332−369), predominantly forms dimers even at a considerably low concentration. Although we could not perfectly rule out a possibility that peptide III would form α-helix-rich dimeric structure other than coiled coil, with these results on the peptide fragments together with the above-mentioned theoretical prediction and CD spectra of K349 and K379, we conclude that this is the neck region of kinesin which dimerizes due to α-helical coiled-coil formation.

Alignment Mode of the Coiled-Coil Fragment. Fluorescence energy transfer measurement can be used to estimate the distance between a fluorescence donor and an acceptor. In order to clarify whether the coiled coil of peptide III is parallel or antiparallel, fluorescence-labeled [Cys^{363}]-peptide III (peptide IIIC) was synthesized. The position of Cys^{363} is so close to the C-terminus of peptide IIIC that the distance between two Cys^{363} of a coiled coil is expected to be close or far depending upon whether the alignment mode is parallel or antiparallel, respectively. Also, since Cys^{363} exists at the *f* position of heptad assignment, it would have little direct interaction with the other peptide of the coiled coil and, therefore, little influence on the coiled-coil formation.

CD spectra of the labeled peptides, IIIC-BIPM and IIIC-NAM, showed α-helix-rich patterns identical to that of peptide III, indicating that there were no significant changes in the secondary structure by the Cys substitution and its labeling with a fluorescent dye. A mixture of IIIC-BIPM and IIIC-NAM also gave a similar CD spectrum.

The fluorescence spectrum of IIIC-BIPM had an emission maximum at 362 nm when excited at 310 nm, whereas IIIC-NAM exhibited no fluorescence emission at 362 nm. A 1:1 mixture of IIIC-BIPM and IIIC-NAM gave weaker emission (77%) at 362 nm than IIIC-BIPM alone (Figure 6). The weakened emission was likely due to fluorescence energy transfer from the BIPM group to the NAM group, because the fluorescence spectrum of IIIC-BIPM overlapped considerably with the absorption spectrum of IIIC-NAM, the maximum of which is at 358 nm.

If the coiled coil would be formed at random among the equimolar mixture of the BIPM- and NAM-labeled peptides, the population of coiled coil consisting of one BIPM- and one NAM-labeled peptide would be expected to be 50%. Therefore, the efficiency of energy transfer, E_T, could be estimated as $(100 - 77)/(100 - 50) = 0.46$. By means of Förster's equation for fluorescence energy transfer, the distance, *r*, between a fluorescence donor and an acceptor group is expressed as $r^6 = R_0^6(1 - E_T)/E_T$, where R_0 is the

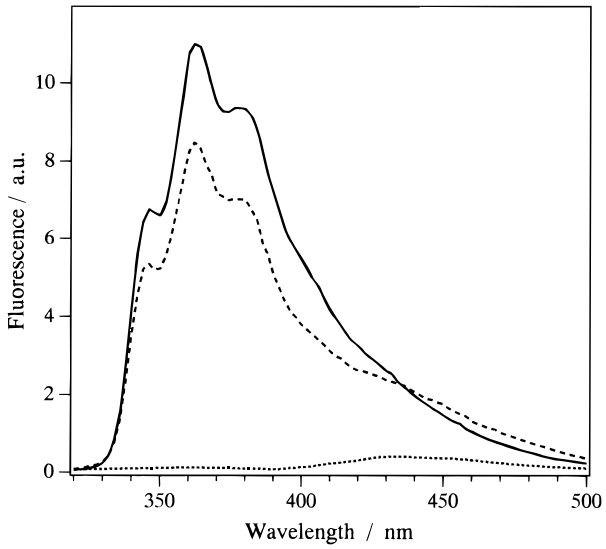

FIGURE 6: Fluorescence spectra of IIIC-BIPM (solid line), IIIC-NAM (dotted line), and their equimolar mixture (dashed line). The peptide concentration was 1 μM for IIIC-BIPM and IIIC-NAM. The mixture containing 1 μM IIIC-BIPM and 1 μM IIIC-NAM was prepared by combining both aqueous solutions without buffer components. The fluorescence spectra were measured in 50 mM potassium phosphate (pH 7.0) with the excitation wavelength at 310 nm.

distance corresponding to $E_T = 0.5$. On the basis of the observed fluorescence and absorption spectra, R_0 is estimated to be 1.89 nm (see Materials and Methods). By substituting 0.46 for E_T, the above equation yields 1.94 nm for the distance, r, between the BIPM and the NAM group of heterodimeric peptide IIIC. The X-ray crystallographic data of GCN4, which is a parallel coiled-coil peptide, shows that the distance between the third atoms from backbone of corresponding *f*-position residues is 1.91 ± 0.08 nm (O'Shea et al., 1991). This value would be comparable to the distance between maleimide groups labeling the cysteine residues of peptide IIIC in a parallel alignment. The chromophores of BIPM and NAM may be a little further than this distance. On the contrary, the corresponding distance of the antiparallel alignment would be 4.2 nm, which would result in only 0.008 for the E_T value. Consequently, it was concluded that the coiled coil of peptide IIIC does not exist in antiparallel alignment but is in a parallel orientation.

Kinetic Stability of the Coiled Coil. In the course of the experiments on the helix−helix alignment, it was demonstrated that the coiled coil of peptide IIIC was extremely stable and exhibited little helix−helix exchange. Mixing a solution (pH 7) of IIIC-BIPM (1 μM) and that of IIIC-NAM resulted in no fluorescence energy transfer. This indicated that no exchanges occurred between IIIC-BIPM and IIIC-NAM homodimers. Even 24 h after mixing or at a much higher peptide concentration (300 μM), the formation of a heterodimeric coiled coil could not be detected in a neutral solution. Thus, the coiled coil of peptide IIIC once folded in a buffer solution is stable and does not interfere with another coiled coil. Also, the dimer dissociation rate constant appears to be extremely small so as not to permit helix exchange. The formation of heterodimeric coiled coil was detected only when IIIC-BIPM and IIIC-NAM were mixed at high concentrations and at a low ionic strength.

Denaturation of Neck Region Fragment. Denaturation curves of peptide III (22 μM) were obtained by titration

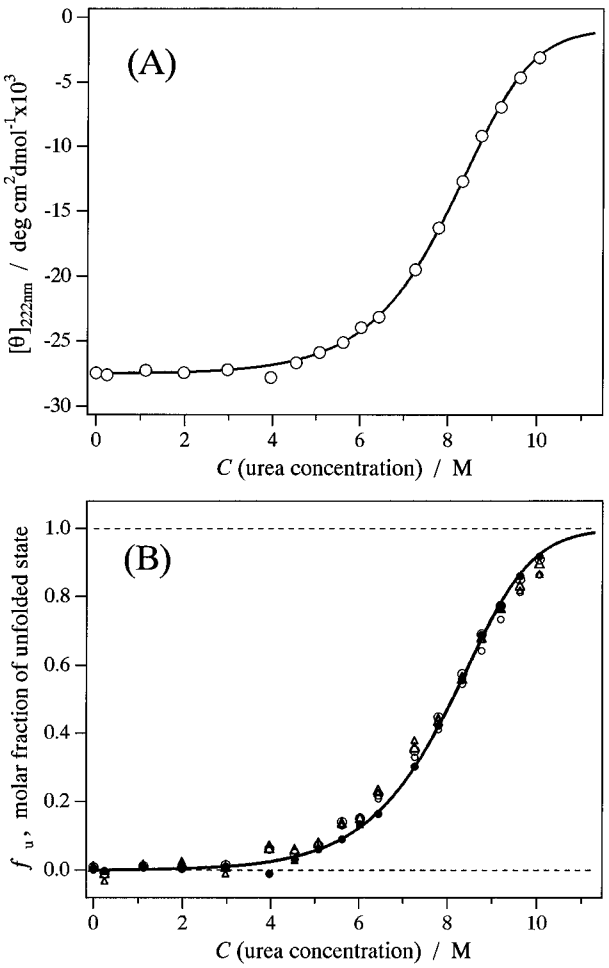

FIGURE 7: (A) Denaturation of peptide III by urea monitored by the molar ellipticity at 222 nm. Circular dichroism of 22 μM peptide III was measured in 20 mM MOPS (pH 7.0) and 0.5 M NaCl containing various concentrations of urea. The data obtained (circles) were fitted with a theoretical curve (solid line) of the transition from dimer to monomer as described in the text. (B) Molar fractional changes of the peptide III denatured by urea. The same peptide III solutions used for CD measurements (A) were also used for the measurements of fluorescence. The ordinate indicates fractions of denatured state calculated on the basis of monomer−dimer equilibrium. The denatured fractions calculated with fluorescence intensities at 310, 330, 340, and 360 nm are represented with small circles, large circles, large triangles, and small triangles, respectively. That from molar ellipticity at 222 nm is shown with closed circles. In the curve-fitting calculation, both native and denatured states were assumed to be linear with respect to urea concentration. The equation for the transition is expressed in the text.

with urea as denaturant (Figure 7). The molar ellipticity at 222 nm gave a sharp transition at 8.1 M urea, and was almost 0 at a higher urea concentration. The transition curve could be fitted to a two-state model with an assumption of a linear relationship between urea concentration, C, and free energy change of denaturation, ΔG, as in the following:

$$\Delta G = -RT \ln (2Pf_u^2/f_f) = \Delta G_{H_2O} - mC$$

where P is peptide concentration; f_u, fraction of unfolded state; f_f, fraction of folded state; ΔG_{H_2O}, ΔG value in water; and m, concentration dependence of ΔG (Pace, 1986; DeFrancesco et al., 1991). The transition parameters, ΔG_{H_2O} and m, were estimated to be 57.7 kJ mol^{-1} and 3.9 kJ mol^{-1} M^{-1}, respectively, by least squares fitting calculations with

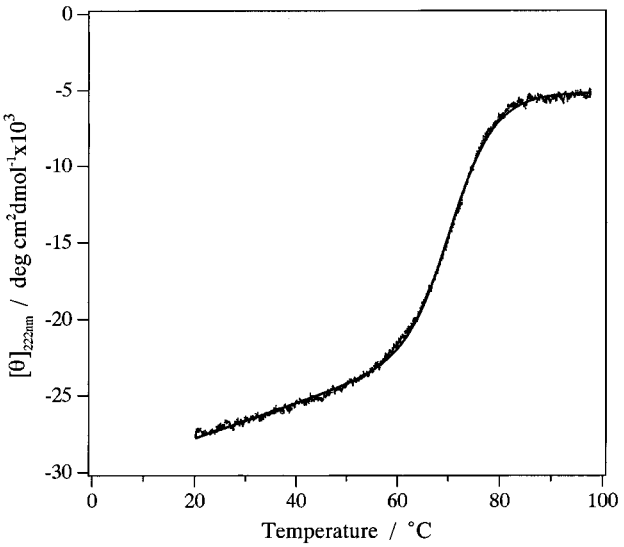

FIGURE 8: Thermal transition of peptide III. The molar ellipticity of 22 μM peptide III at 222 nm was monitored in 20 mM MOPS (pH 7.0) and 0.5 M NaCl with increasing temperature at a rate of 0.8 K/min. The data observed (dots) were fitted with a theoretical curve (solid line). The curve-fitting calculation was performed using the following equations: $K = 2\ Pf_u^2/f_f$ and $d(\ln K)/dT = \Delta H^{vH}/RT^2$, where K is the dissociation constant; T, temperature; ΔH^{vH}, van't Hoff enthalpy; and R, gas constant; the others are described in the text. The latter equation was transformed to $\ln K = (\Delta H^{vH}/R)(1/T_m - 1/T) + \ln P$, where T_m is the transition temperature.

the above equation (Figure 7A). The energy difference between the folded and unfolded states thus estimated would be 9.5×10^{-20} J/molecule. Hydrolysis of ATP releases 5.1×10^{-20} J/molecule. Direct single molecular observation of kinesin movement gave mechanical data such as an 8 nm step size with a 4 pN force (Kojima et al., 1996). These would correspond to kinetic energy of 3.2×10^{-20} J. Interestingly, our estimation is close to these energy values.

The unfolding course by urea was also monitored with fluorescence emission of tryptophan and tyrosine residues upon excitation at 275 nm. The emission maximum shifted from 341 to 352 nm with increasing urea concentration up to 10 M. The emission maximum being at 341 nm could be interpreted as most tryptophan residues existing in a hydrophobic environment in the coiled coil. This would support the assignment of the coiled-coil region and its heptad coding described in the previous section. The fractional change derived from fluorescence intensity at each wavelength along the emission peak coincided with that from molar ellipticity (Figure 7B). Accordingly, it is concluded that the denaturation of the hydrophobic core was linked with that of secondary structure. It should be noted that the transition exhibited no apparent intermediate state. Trp^{340} and Trp^{368}, which exist at *d* positions of heptad near the two termini of peptide III, appeared to become exposed simultaneously.

A thermal denaturation curve of 22 μM peptide III is shown in Figure 8. It could be interpreted as a simple two-state transition. The transition temperature, which generally depends on the peptide concentration for an association system, was 71°C. The van't Hoff enthalpy was estimated to be 329 kJ mol^{-1} at the transition temperature. The equilibrium denaturation experiments by urea and heat have led us to reach the conclusion that despite the existence of intervening hydrophilic residues (see above) the coiled coil of peptide III is likely to consist of a single domain.

CONCLUSIONS

Using several synthetic peptide fragments in the region of kinesin (315−379) together with the statistical prediction methods, the first coiled-coil region, the neck region of kinesin, was identified to be the sequence of Asn^{332} to Arg^{369}. The fragment (332−369) formed a stable dimer even at a concentration in μM range. The deletion of either half of the fragment resulted in much poorer dimerization ability. These results are also compatible with the difference of K349 being monomeric and K379 being dimeric. The structure of the dimeric (332−369) was proved to be a parallel α-helical coiled coil by means of CD, sedimentation equilibrium, and fluorescence energy transfer measurements. In the neck region sequence, hydrophilic Glu^{347} and Asn^{351} at *d* and *a* positions, respectively, would induce the parallel helix−helix alignment to prevent unfavorable pairing of these hydrophilic residues and hydrophobic core residues in antiparallel form.

The coiled coil of the neck region was stable not only thermodynamically but also kinetically. In buffer solutions, the coiled-coil peptides exhibit no detectable exchange of monomers nor do they form associated multimers. This feature is important for the kinesin function, as it should act as a dimer. In summary, the dimeric structure of kinesin is specified even by the neck region fragment alone.

The denaturation experiments revealed that the neck region fragment consisted of a single domain at least in a thermodynamical manner. The unfolding process of the coiled-coil fragment was considered as turning into disordered secondary structure and, simultaneously, dissociation of the dimer. Possible mechanical participation of this neck region in kinesin functions would be of particular importance (Hirose et al., 1996). The three-dimensional structure of this region in solutions would also be especially interesting, and studies for such an elucidation are now in progress.

NOTE ADDED IN PROOF

After acceptance of this paper, we learned that B. Tripet, R. D. Vale, and R. S. Hodges had worked on similar peptides and obtained results consistent with ours (Tripet et al., 1997).

ACKNOWLEDGMENT

We sincerely thank Dr. Ronald D. Vale (University of California, San Francisco) and Dr. Robert S. Hodges (University of Alberta, Canada) for critical reading and for valuable discussion. We are also grateful to Dr. J. Kull (University of California, San Francisco) for supplying the plasmids for K349 and K379. The secretarial assistance of Ms. Akemi Kamiya is greatly acknowledged. This work was supported by grants-in-aid from the Agency of Industrial Science and Technology, MITI.

APPENDIX

Prediction of Amphipathic Helical Propensity[2]

Amphipathic helices can be found in various supersecondary structures such as coiled coils and helix bundles. Most

[2] Contributed by Hisayuki Morii, National Institute of Bioscience and Human-Technology, Tsukuba, Ibaraqi 305, Japan.

double-stranded coiled coils are amphipathic, and the detailed characteristics of coiled-coil structure have been investigated (Hodges, 1992, 1996; Adamson et al., 1993, and references cited therein). Generally, the amphipathic α-helical sequences to form coiled-coil or helix-bundle structures are characterized with the heptad assignment, i.e., *a*, *b*, *c*, *d*, *e*, *f*, and *g*, in which *a* and *d* positions are assigned to the core of the coiled-coil and are in most cases hydrophobic residues (McLachlan et al., 1975). The propensity of the amphipathic helix is related to the stability of its supersecondary structure, which mainly depends on heptad amphipathic periodicity (Bryson et al., 1995). Additionally, the stability is affected by intrinsic helical propensity, inter- and intrahelix electrostatic interactions, and packing of hydrophobic side chains (Adamson et al., 1993; Hodges, 1992).

Herein, a novel method to assess amphipathic helical propensity has been developed on the basis of energetical evaluation as follows. The heptad assignment for coiled coils can be classified into two categories, i.e., *a* and *d* positions and the others (*b*, *c*, *e*, *f*, *g*), which are referred to as the "core" and "outfield" positions, respectively. For each amino acid, two basic scores are given corresponding to the core and outfield positions. The basic scores, G_a, are given as follows: Leu (−1.72, 0), Ile (−1.86, 0), Val (−1.36, 0), Met (−1.38, 0), Phe (−1.36, 0), Tyr (−1.01, 0), Gly (0, 0), Ala (−0.42, 0), Lys (0, −1.95), Arg (0, −1.77), His (−0.18, 0), Glu (0, −1.07), Asp (0, −1.05), Gln (0, −0.50), Asn (0, −0.82), Ser (0, −0.05), Thr (−0.35, 0), Cys (−0.48, 0), Trp (−1.01, 0), and Pro (−0.98, 0), the two values of which in each set of parentheses are those of core and outfield, respectively.

These scores are originally adopted from the energy changes ΔG_{obs} in transferring the side chains from octanol to water environment (Fauchere et al., 1983). Since it is thought that both hydrophobic residues at the core and hydrophilic residues at the outfield contribute to the stabilization of the coiled coil, they are given negative energy values ($-\Delta G_{obs}$ for the former and ΔG_{obs} for the latter). For the other cases, i.e., hydrophobic residues at the outfield and hydrophilic residues at the core, the scores were set to be 0 as reference states. Although the destabilizing effects, e.g., those of Leu and Ala at the outfield, should not be the same, the difference is assumed to be small, and the values for them have been set to be 0. These original scores were further modified in the following way. By molecular modeling it is assumed that the side chains of the coiled-coil region are not fully exposed to the solvent in contrast with those of amino acid monomers. Thus, the differences in the scores of core and outfield for Leu and Ile are corrected to have reduced values by 0.6 kcal mol^{-1}, ΔG_{obs} of the methylene group. Similarly, for Val, Met, Tyr, Lys, Arg, Glu, and Gln, the differences between the two states are reduced by 0.3, 0.3, 0.3, −0.6, −0.4, −0.2, and −0.2 kcal mol^{-1}, respectively. The score difference of Cys is estimated to be smaller than that of Met by 1.2 kcal mol^{-1}, equivalent to two methylene groups. Our preliminary study shows that the aromatic residues at the core would have a smaller stabilization energy for coiled-coil formation than Leu in spite of their larger ΔG_{obs}, so that the score for Phe is set to be the same as that for Val (Morii et al., 1995). Since Trp makes coiled coils more unstable than Phe, the score for Trp is chosen to be the same as that for Tyr.

Table 2: Model Calculation of the Prediction for Amphipathic Helices

model	sequence	score of predominant heptad frame[a] averaged[c]	score of predominant heptad frame[a] peak[d]	score of secondary class[b] averaged[c]
1	$(LLLLLLL)_n$	2.34 (7)	2.68	
2	$(LLLLLEL)_n$	2.93 (5)	3.30	1.53 (2)
3	$(LLELLEL)_n$	3.66 (4)	4.08	1.71 (2)
4	$(LEELLEL)_n$	4.59 (3)	5.03	1.92 (2)
5	$(LEELLEE)_n$	5.74 (2)	6.21	2.14 (2)
6	$(LEELEEE)_n$	7.19 (1)	7.67	2.40 (2)
7	$(LEEEEEE)_n$	2.68 (2)	3.06	1.00 (5)
8	$(EEEEEEE)_n$	1.00 (7)		
9	$(LE)_n$	2.14 (7)	2.48	
10	$(LEE)_n$	1.85 (7)	4.36	

[a] The score, *w*, for the most probable type of heptad frame shift is represented. [b] The scores of the second most probable ones are listed. [c] The scores are averaged along the sequence. The multiplicity for the types of heptad frame shift are expressed in the parentheses. [d] The maximum scores are listed.

So as to prevent fully hydrophilic sequences from gaining the scores preferable for coiled coil, the scores at the outfield are modified by multiplying by the nondimensional factor $G_c/(-2$ kcal mol$^{-1})$, where G_c represents the averaged score of two nearest core positions. This modification can make the heptad amphipathic periodicity more obvious. The score of each position is calculated by (i) assigning the sequence to one of the seven possible heptad repeat frames; (ii) giving each residue the basic score G_a corresponding to the position, core or outfield; (iii) modifying G_a at outfield positions with $G_c/(-2)$ as above; (iv) averaging the scores geometrically in the window of 15 residues; and (v) converting the scores of free energy to the statistical weight factors at 20 °C using the equation $w = \exp(-G_a^{av}/RT)$. Seven scores for each position are obtained according to seven types of heptad frame shift. The type of heptad frame shift is expressed with the residue number assigned to *a* positions as $7N-i$, where *N* denotes a positive integer and *i* is an integer as $0 \leq i \leq 6$; for example, assignment of the residues, 348, 349, ..., and 354, to *a*, *b*, ..., and *g*, is expressed as $7N-2$.

In order to confirm the validity and versatility of this method, several sequential heptapeptides are tested at first. As listed in Table 2, the typical amphipathic periodicity of coiled coils, coded here as model 6, gives a significantly high score and the predominant heptad frame shift is single. As the ratio of Leu to Glu increased from model 6 to model 1, the scores of the predominant heptad frame shifts decreased and their multiplicity increased. The multiplicity of the predominant ones reflects the width of the hydrophobic face on helices, which may affect the number of helices bundled up into coiled coils or helix bundles. The threshold level to distinguish amphipathic helices from the others seems to be 3.0, because this is the border between models 2 and 3, or 6 and 7. The application for sequential di- and tripeptides results in only low averaged scores with wavy profiles (Table 2). The periodicity of these two peptides is not suitable for amphipathic helix formation.

The application of this method to tropomyosin a chain, which is known as a typical coiled-coil protein, showed that it is a single-domain coiled coil with a high score except for the sequence around (20−30). Similarly, light meromyosin gives the result that almost entirely along its length it forms coiled coils made up of mainly four domains. For cyto-

chrome b_{562} and myohemerythrin, four helix bundle proteins, three out of four major helices are predicted. On the other hand, for hemoglobin, a globular α-helical protein, and bacteriorhodopsin, an α-helical membrane protein, the maximal scores are not high and the multiplicity is high. These features suggest that they resemble the model types 3−5 listed in Table 2. These results of the examples well prove the validity of this method.

Finally, it should be mentioned that this method is effective in estimating the propensity of amphipathic helices and is different from the method of Lupas et al. (1991), which is effective for searching the sequences homologous to natural coiled-coil proteins. Therefore, this method would be useful, for example, to find coiled coils not homologous to natural ones but thermodynamically stable.

REFERENCES

Adamson, J. G., Zhou, N. E., & Hodges, R. S. (1993) *Current Opin. Biotechnol. 4*, 428−437.

Berger, B., Wilson, D. B., Wolf, E., & Tonc, T. (1995) *Proc. Natl. Acad. Sci. U.S.A. 92*, 8259−8263.

Bloom, G. S., & Endow, S. A. (1994) *Protein Profile 1*, 1059−1105.

Bryson, J. W., Betz, S. F., Lu, H. S., Suich, D. J., Zhou, H. X., O'Neil, K. T., & DeGrado, W. F. (1995) *Science 270*, 935−941.

Chen, Y.-H., Yang, J. T., & Chau, K. H. (1974) *Biochemistry 13*, 3350−3359.

Correia, J. J., Gilbert, S. P., Moyer, M. L., & Johnson, K. A. (1995) *Biochemistry 34*, 4898−4907.

de Cuevas, M., Tao, T., & Goldstein, L. S. B. (1992) *J. Cell Biol. 116*, 957−965.

DeFrancesco, R., Pastore, A., Vecchio, G., & Cortese, R. (1991) *Biochemistry 30*, 143−147.

Fauchere, J.-L., & Pliska, V. (1983) *Eur. J. Med. Chem.−Chim. Ther. 18*, 369−375.

Förster, T. (1948) *Ann. Phys. (Leipzig) 6* (2), 55−75.

Gilbert, S. P., Webb., M. R., Brune, M., & Johnson, K. A. (1995) *Nature 373*, 671−676.

Goldstein, L. S. B. (1993) *Annu. Rev. Genet. 27*, 319−351.

Hackney, D. D. (1994) *Proc. Natl. Acad. Sci. U.S.A. 91*, 6865−6869.

Hirokawa, N., Pfister, K. K., Yorifuji, H., Wagner, M. C., Brady, S. T., & Bloom, G. S. (1989) *Cell 56*, 867−878.

Hirose, K., Lockhart, A., Cross, R. A., & Amos, L. (1996) *Proc. Natl. Acad. Sci. U.S.A. 93*, 9539−9544.

Hisanaga, S., Murofushi, H., Okuhara, K., Sato, R., Masuda, Y., Sakai, H., & Hirokawa, N. (1989) *Cell Motil. Cytoskeleton 12*, 264−272.

Hodges, R. S. (1992) *Curr. Biol. 2*, 122−124.

Hodges, R. S. (1996) *Biochem. Cell Biol. 74*, 133−154.

Huang, T.-G., Suhan, J., & Hackney, D. D. (1994) *J. Biol. Chem. 269*, 16502−16507.

Kojima, H., Muto, E., Higuchi, H., & Yanagida, T. (1996) *Biophys. J. 70*, A36.

Kull, F. J., Sablin, E. P., Lau, R., Fletterick, R. J., & Vale, R. D. (1996) *Nature 380*, 550−555.

Lilley, T. H. (1985) in *Chemistry and Biochemistry of the Amino Acids* (Barrett, G. C., Ed.) Chapter 21, Chapman & Hall, London.

Lockhart, A., & Cross, R. A. (1994) *EMBO J. 13*, 751−757.

Lupas, A., Dyke, M. V., & Stock, J. (1991) *Science 252*, 1162−1164.

Ma, Y.-Z., & Taylor, E. W. (1995a) *Biochemistry 34*, 13233−13241.

Ma, Y.-Z., & Taylor, E. W. (1995b) *Biochemistry 34*, 13242−13251.

McDonald, H. B., Stewart, R. J., & Goldstein, L. S. B. (1990) *Cell 63*, 1159−1165.

McLachlan, A. D., & Stewart, M. (1975) *J. Mol. Biol. 98*, 293−304.

Morii, H., Ishimura, M., Honda, S., & Uedaira, H. (1995) *Pept. Chem. 1994*, 445−448.

O'Shea, E. K., Klemm, J. D., Kim, P. S., & Alber, T. (1991) *Science 254*, 539−544.

Pace, C. N. (1986) *Methods Enzymol. 131*, 266−280.

Provencher, S. W. (1982) *Comput. Phys. Commun. 27*, 213−227.

Sablin, E. P., Kull, F. J., Cooke, R., Vale, R. D., & Fletterick, R. J. (1996) *Nature 380*, 555−559.

Shimizu, T., Sablin, E., Vale, R. D., Fletterick, R., Pechatnikova, E., & Taylor, E. W. (1995) *Biochemistry 34*, 13259−13266.

Solli, N. J., & Herskovits, T. T. (1973) *Anal. Biochem. 54*, 370−378.

Stryer, L. (1978) *Annu. Rev. Biochem. 47*, 819−846.

Tripet et al. (1997) *J. Biol. Chem.* (in press).

Vale, R. D., Reese, T. S., & Sheetz, M. P. (1985) *Cell 42*, 39−50.

Vale, R. D., Funatsu, T., Pierce, D. W., Romberg, L., Harada, Y., & Yanagida, T. (1996) *Nature 380*, 451−453.

Walker, R. A., & Sheetz, M. P. (1993) *Annu. Rev. Biochem. 62*, 429−451.

Walker, R. A., Salmon, E. D., & Endow, S. A. (1990) *Nature 347*, 780−787.

Yang, J. T., Laymon, R. A., & Goldstein, L. S. B. (1989) *Cell 56*, 879−889.

Yang, J. T., Saxton, W. M., Stewart, R. J., Raff, E. C., & Goldstein, L. S. B. (1990) *Science 249*, 42−47.

BI962392L